Scanning Microscopy

Volume 4 | Number 1 Article 4

12-25-1989

Backscattered Electron Imaging of Partially-Demineralized Enamel

D. G. A. Nelson
The Procter & Gamble Co.

Follow this and additional works at: https://digitalcommons.usu.edu/microscopy

 Part of the Biology Commons

Recommended Citation

Nelson, D. G. A. (1989) "Backscattered Electron Imaging of Partially-Demineralized Enamel," *Scanning Microscopy*: Vol. 4 : No. 1 , Article 4.
Available at: https://digitalcommons.usu.edu/microscopy/vol4/iss1/4

This Article is brought to you for free and open access by the Western Dairy Center at DigitalCommons@USU. It has been accepted for inclusion in Scanning Microscopy by an authorized administrator of DigitalCommons@USU. For more information, please contact digitalcommons@usu.edu.

Scanning Microscopy, Vol. 4, No. 1, 1990 (Pages 31-42) 0891-7035/90$3.00+.00
Scanning Microscopy International, Chicago (AMF O'Hare), IL 60666 USA

BACKSCATTERED ELECTRON IMAGING OF PARTIALLY-DEMINERALIZED ENAMEL

D. G. A. Nelson

The Procter & Gamble Co.
P.O. Box 398707
Cincinnati, Ohio 45239
Telephone: (513)-245-2131

(Received for publication August 23, 1989, and in revised form December 25, 1989)

Abstract

Backscattered electron (BE) microscopy is being used increasingly as a technique to study the dissolution of dental enamel because of its high resolution and relatively easy sample preparation. Subsurface details such as striae of Retzius, cross-striations and prism microstructure have been observed with a resolution better than 0.1 micrometers using this technique. Since BE images of demineralized enamel appear very similar to microradiography images, it is tempting to interpret them in a similar fashion. We attempt to show that the interpretation of BE images is not straightforward because enamel is not a homogeneous one-phase material, but a two-component composite material consisting of variable amounts of apatite mineral and organic matter. During re- and demineralization, other calcium phosphate phases may precipitate to further complicate the interpretation of the images. BE images of partially demineralized enamel are affected by local variations in the protein / mineral ratio and also by the reprecipitation of other calcium phosphate phases. BE images are not mineral density maps, but are mean atomic number maps.

Key Words: Atomic Number Maps, Backscattered Electrons, Caries, Demineralization, Dental Enamel, Fluoride, Mineral Density Maps, Monte Carlo Calculations, Subsurface Lesions.

Introduction

Caries is a process which initially results in subsurface demineralization of dental enamel. Histological studies of carious enamel using polarized light microscopy have identified four distinct regions or zones. They are, moving inwards from the surface, the surface zone, the lesion body, the dark zone and the translucent zone. The histology of subsurface lesions has been described in detail in the past (Silverstone, 1973; Shellis and Hallsworth, 1987), but the distinctive features of each zone are discussed briefly.

The surface zone has a mineral content higher than the underlying enamel in the lesion body, and lower than undemineralized surface enamel. Most of the demineralization occurs in the lesion body, where the mineral content can be as low as 20 vol percent. Apatite crystals in this zone are often partially dissolved, but at the prism peripheries, next to the prism junctions, large crystals, presumably formed by remineralization, can be found. The next zone is called the dark zone because of its appearance in polarized light microscopy. There is evidence of some remineralization phenomena occurring there (Silverstone, 1977). The advancing front of the lesion is called the translucent zone which is characterized mainly by mineral loss at the prism junctions.

Re- and demineralization processes in human carious enamel have been routinely studied using quantitative microradiography (Groeneveld, 1974; Arends and Gelhard, 1983; White, 1988), which produces a map of the mineral density in a lesion with a resolution of 2-5 micrometers. This technique makes it possible to determine the net re- or demineralization in a lesion relative to control lesions. The technique requires that specimens are prepared in the form of plano-parallel sections approximately 50-100 micrometers thick. Therefore, because microradiography is a projection technique and because information is summed or averaged over the thickness of the section, details of re- and demineralization processes at the prism level are normally blurred and cannot be observed. Recently, an effort was made to improve the quality and resolution of microradiographs of demineralized enamel using monochromatic synchrotron radiation combined with an X-ray image magnifier (Takagi et al., 1984).

Normally, in scanning electron microscopy (SEM), images are formed using secondary electrons (SEs) produced by interactions of the primary electron beam with a thin (approximately 10-20 nm

thick) surface coating of Au or Pt. These images usually reflect the surface topography of the specimen. However, after the primary electrons penetrate the surface they are involved in multiple elastic and inelastic scattering events with atoms in the sample (Joy, 1988). As a consequence, a proportion of the incident primary electrons, the backscattered electrons (BEs), are deflected back out of the specimen. Because the BEs have a much higher energy than SEs, they can be discriminated from SEs with a suitable detector. More importantly, because the primary electrons are scattered more effectively by higher atomic number atoms, BE images contain subsurface detail that reflects changes in the relative composition of the material.

BE images of demineralized enamel which contain features unseen in microradiographs have been reported recently by several workers (Boyde and Jones, 1983; Jones and Boyde, 1987; Pearce and Nelson, 1989). These images are remarkably similar to microradiographs of subsurface lesions but contain microstructural detail at the prism level. For example, subsurface compositional detail related to Striae of Retzius, cross striations and prism peripheries are "disclosed" in BE images of demineralized enamel.

The purpose of this review is to show the versatility of the BE imaging technique in following de- and remineralization processes in human dental enamel and to more fully explore the fundamental reasons for variation in the contrast of BE images of demineralized enamel. We used Monte Carlo methods to calculate BE coefficients for several different models of partially demineralized enamel in order to understand the reasons for the detail in the BE images.

Materials and Methods

Sample Preparation

Approximately 150 demineralized human and bovine enamel chips have been examined in the SEM using BE imaging. Natural lesions from extracted deciduous molars and permanent premolars were sectioned transversely through the lesions. Each hemisectioned sample was embedded in epoxy resin and the sectioned face, perpendicular to the natural surface, was serially polished.

Pre-polished enamel chips which had been subjected either to intra-oral caries testing or in vitro de- and remineralization testing were cleaned with detergent in preparation for examination by BE imaging. Lesion formation in these samples was also followed by examining transverse sections in a similar fashion to that done for the natural lesions.

The serial polishing procedure consisted of grinding an enamel facet on plate glass with a slurry of 12.5 micrometers and then 5 micrometers aluminum oxide. This was followed by polishing with 6 and 1 micrometers diamond lapping compound on artificial silk. The samples were cleaned with distilled water between each operation in an ultrasonic bath.

Intra-oral Caries Testing

Sound human enamel chips were mounted in lower-arch acrylic appliances and subjected to in vivo intra-oral caries testing as described in detail elsewhere (Pearce and Gallagher, 1979). The polished enamel surfaces were covered with Terylene® gauze to enhance the growth of plaque. The appliances with the plaque-covered enamel chips were immersed 4 times daily in 0.28 M glucose solution for periods of up to 10 mins. The appliances were removed during normal oral hygiene procedures. After 5 days, a distinct surface softening 10-30 micrometers deep was produced. At the end of the experiment, the enamel chips were recovered, cleaned with detergent, and prepared for SEM examination. Some chips were hemi-sectioned transversely through the lesion and polished, whereas other exposed surfaces were examined directly by SEM.

In Vitro Demineralization

Polished human enamel chips approximately 3 x 2 mm in area were embedded in epoxy resin and immersed in 40 ml of demineralizing solution at 37°C without agitation. The demineralizing solution consisted of 0.1 M lactic acid at pH 4.5 plus 0.2 mM sodium methane diphosphonate (MHDP) which is a surface dissolution inhibitor (Featherstone et al., 1979). The polished chips were withdrawn for SEM examination after 1, 2, 6, 12 and 48 hrs.

In Vitro pH Cycling

Intact human enamel premolars and molars were cleaned with warm water and detergent, washed with deionized water and dried in air. Each tooth was painted with an acid-resistant varnish leaving an upper and lower window, approximately 1x3 mm, on each buccal or lingual enamel surface. The daily treatment routine consisted of one demineralization period, one remineralization period, and two topical treatments, one before demineralization and one before remineralization.

1) Demineralization: The samples were given 17 h demineralization in 40 ml of acid buffer (37°C) containing 2.0 mmol/l Ca, 2.0 mmol/l PO_4, 0.075 mol/l acetate at pH 4.3;

2) Remineralization: The samples were bathed for 6 h in 20 ml of a pH 7.0 mineralizing solution (37°C) containing 1.5 mmol/l Ca, 0.9 mmol/l PO_4, 0.15 mol/l KCl, and 20 mmol/l cacodylate buffer;

3) Topical treatments: Before and after a topical treatment, the teeth were removed from the re- or demineralizing solutions and thoroughly washed with deionized water. For the dentifrices, a 1:3 (w/w) fresh slurry was made in double distilled water every time within 1/2 h of use. The samples were immersed in 4 ml of the slurry for 1 min while being agitated on an orbital shaker. Samples were then immersed in 4 ml of the mouthrinse without any dilution. Control samples were not immersed at all.

Daily cycles of de- and remineralization continued for 6 days plus one weekend at the end of the experiment when the samples were then placed in the remineralizing solution.

Treatments included (1) a control group receiving de- and remineralization cycles, but no topical fluoride treatment; (2) a 0.243% NaF dentifrice with silica abrasive containing 1,100 ppm F^- (Advanced Formula Crest, Procter and Gamble Co., USA); (3) a 0.7% sodium monofluorophosphate (MFP) dentifrice with dicalcium phosphate dihydrate abrasive containing 1,000 ppm F^- (Regular Colgate); (4) a NaF mouthrinse containing NaF at 0.05 % wt/vol, with 225 ppm F^- (Fluorigard, Colgate-Hoyt).

Monte Carlo Calculations

The interaction of the primary electron beam with bulk enamel was simulated using the single scattering Monte Carlo model and a program written by Joy (1988). This model and the program are described in detail elsewhere (Joy, 1988) but basically, only elastic scattering events are assumed

to determine the path taken by an electron, whereas energy loss is assumed to be continuous and not to be the result of discrete inelastic events. Calculations were performed using the following parameters: 1) an accelerating voltage of 30 keV; 2) 10000 trajectories were used, so the calculations had a standard error of 1%; 3) the mean atomic number, $\bar{Z}$, for stoichiometric hydroxyapatite (HAP), $Ca_{10}(PO_4)_6(OH)_2$, was calculated to be 14.08 and the mean atomic weight $\bar{A}$ was calculated to be 28.34 using the following equations where Z_i, A_i, and c_i are the atomic numbers, the atomic weight, and the weight fraction of atom i respectively.

$$\bar{Z} = \sum_i c_i Z_i \quad (1)$$

$$\bar{A} = \sum_i c_i A_i \quad (2)$$

A density, d, of 3.20 g/cm^3 was used for HAP in the Monte Carlo calculations; and 4) for simulations of a HAP/protein composite, the protein was approximated by $\bar{Z}$ = 6.5, $\bar{A}$ = 13 and d = 1.3 g/cm^3.

Given the mean atomic number and weight plus the density, the Monte Carlo program calculated three important parameters: the BE coefficient, η,

$$\eta = n_{BS}/n_P = i_{BS}/i_P \quad (3)$$

the mean BE energy, and the range. The BE coefficient is defined as the number of backscattered electrons, n_{BS} (or current, i_{BS}), divided by the number of primary beam electrons, n_P (or current, i_P), incident on the sample. The range is related to the extent of the "diffusion cloud" and represents the mean free path of primary electrons in the sample. The precision of the BE data could be improved by always using the same random number sequence in any given set of simulations (D.C. Joy, personal communications). Some additional contrast may arise from the geometry of the BE detector and its size and position relative to the sample should ideally be included in the calculations (D.C. Joy, personal communications). In our experiments, the detector distance and geometry was always held constant relative to the sample. The Monte Carlo calculations also do not take into account the effect of space charge in the surface layer of the sample (A. Boyde, personal communication).

Electron Microscopy

Sound and demineralized human enamel surfaces which had been polished were examined at 30 keV in a Philips 505 SEM. The specimens had been sputter-coated to a thickness of 10-12 nm with gold or carbon. A spot size of 5 nm was used for high-resolution SE images, whereas a spot size of 50 to 100 nm was used for BE images. For BE imaging, the specimens were examined at a working distance of approximately 12 mm.

Results

In the first set of Monte Carlo calculations, called the HAP/voids model, the only parameter allowed to vary for stoichiometric HAP was density. The mean atomic number and weight were kept the same and the calculated BE coefficients did not appear to change significantly (Table 1; Fig. 1). For example, the density of HAP was allowed to vary from 1.5 to 3.3 g/cm^3, simulating materials consisting of varying proportions of voids and HAP. However, the calculated BE coefficients remained within the range of 0.165-0.173 although the primary electron range (related to the size of the primary electron diffusion cloud in the solid) increased with decreasing density (Table 1). Each BE coefficient calculation had a standard error of 0.002. This suggested that there was no significant variation in BE coefficient with density or with volume % HAP in the material. A pure, stoichiometric HAP single crystal has a density of approximately 3.2 g/cm^3 and calculations with lower densities effectively simulate materials consisting of small stoichiometric crystals and voids, but with no protein or organic matter. Examples of such materials would be densely-packed ceramic HAP pellets.

In our next series of calculations we simulated a composite material consisting of stoichiometric HAP and organic matter, called the HAP/protein model. At the simplest level, biological materials such as dental enamel and dentin can be considered as mixtures of 2 materials of different density, HAP and organic matter. The density of the composite, ρ, can be defined as:

$$\rho = f_a \rho_a + (1 - f_a) \rho_b \quad (4)$$

where f_a is the fraction of material a by volume. The following equations were used to convert mass fraction to volume fraction for a 2 material composite, where F_a is the fraction of material a by mass.

$$F_a = f_a / [f_a + (1 - f_a) \rho_b/\rho_a] \quad (5)$$

$$f_a = F_a(\rho_b/\rho_a) / [1 - F_a(1 - \rho_b/\rho_a)] \quad (6)$$

In these simulations, the mineral-to-protein volume ratio was allowed to vary from 100/0 to 38/62. The calculated BE coefficients dropped progressively from 0.173 for pure, stoichiometric HAP with no protein, to 0.132 for a material consisting of approximately 40% volume HAP and 60% volume protein (Table 2., Fig. 1). Dentin consists approximately of 45% volume HAP and 55% protein, so we can now explain why dentin appears darker in BE images than enamel on the basis on these calculated BE coefficients. When we calculated the mean atomic numbers for these hypothetical composite materials, we found that $\bar{Z}$ changed from 14.08 for pure, stoichiometric HAP to 11.05 for the 38/62 HAP/protein material. Because the previous set of calculations showed that density did not affect the BE coefficient, we concluded that in these materials the BE coefficient reflected changes in $\bar{Z}$. In fact, when we plotted our BE coefficients against a previously-reported, empirical, polynomial equation (Reuter, 1972), which related the BE coefficient to $\bar{Z}$, we found a very good fit with our calculated BE coefficients (Fig. 2). We found no difference in the mean BE energy for these materials (Fig. 3), so changes in the energy distribution of the BE electrons did not appear to be a factor in understanding the BE images of demineralized enamel.

The HAP component of sound dental enamel is approximately 87 % by volume or 95 % by weight, the remaining fraction consists of organic matter and water. The organic fraction of enamel is

Monte Carlo Calculations of HAP/Protein Composites. 30 keV; 10,000 Electron Trajectories.

Figure 1. Calculated BE coefficients plotted against density for the HAP/voids model and the HAP/protein model. Boxed regions refer to the approximate compositions of sound dental enamel and dentin.

Figure 2. Calculated BE coefficients plotted against HAP/protein composition compared with empirical polynomial relating Z to BE coefficient.

Figure 3. Mean BE energy plotted against density for the HAP/voids model and the HAP/protein model.

Table. 1. Monte Carlo Calculations of HAP/Voids Composite

Volume Fraction of HAP	Density g/cm^3	BSE Coefficient (±0.002)	Range (micrometers)	Mean BSE Energy (eV)
1.03	3.3	0.172	7.36	19.18
1.00	3.2	0.173	7.59	19.15
0.97	3.1	0.171	7.84	19.24
0.94	3.0	0.165	8.10	19.14
0.91	2.9	0.166	8.38	18.83
0.88	2.8	0.166	8.68	19.28
0.84	2.7	0.169	9.00	19.35
0.81	2.6	0.166	9.35	19.04
0.78	2.5	0.168	9.72	18.98
0.72	2.3	0.166	10.56	18.81
0.66	2.1	0.169	11.57	19.34
0.59	1.9	0.165	12.79	19.42
0.53	1.7	0.167	14.29	18.78
0.47	1.5	0.171	16.20	19.39

Table. 2. Monte Carlo Calculations of HAP/Protein Composite

Mass Fraction of HAP	Volume Fraction of HAP	Mean Atomic Number	Density g/cm^3	BSE Coefficient (±0.002)	Range (micrometers)
1.00	1.00	14.08	3.20	0.173	7.59
0.95	0.89	13.70	3.11	0.168	7.77
0.90	0.79	13.32	3.01	0.159	7.99
0.85	0.70	12.94	2.92	0.153	8.20
0.80	0.62	12.56	2.82	0.151	8.45
0.75	0.55	12.18	2.73	0.142	8.69
0.70	0.49	11.81	2.63	0.144	8.98
0.65	0.43	11.43	2.54	0.137	9.25
0.60	0.38	11.05	2.44	0.132	9.58

approximately 1-2% by weight and consists mainly of protein and lipid, leaving 3-4 wt % of water. If we assume that during the demineralization processes occurring during subsurface lesion formation none of the organic component is lost and that only the mineral component partially dissolves, then the ratio of organic to inorganic components increases slightly in the demineralized enamel. In an electron microscope, enamel is dehydrated and the water fraction can be ignored. If the mineral component is assumed to be stoichiometric HAP and the organic component 1.5% by weight, then there will be small decreases in mean atomic number and mean atomic weight for this model of demineralized, dehydrated enamel. The Monte Carlo calculations show (Table 3) that this model appeared to produce either very small or statistically insignificant decreases in the BE coefficient from 0.173 for pure stoichiometric HAP to 0.163 for a material consisting of approximately 38% volume HAP and a HAP mass fraction of 0.976. These changes in the calculated BE coefficients were much less than the protein/HAP model described above and did not appear to explain the contrast seen in the BE images of demineralized enamel.

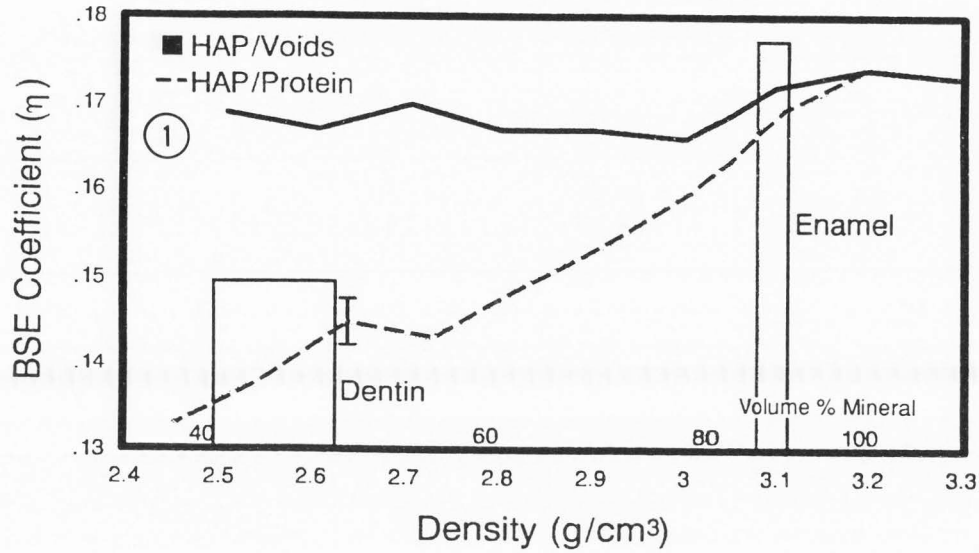
HAP/Voids
HAP/Protein
1
Enamel
Dentin
Volume % Mineral
40
60
80
100
BSE Coefficient (η)
.18
.17
.16
.15
.14
.13
2.4
2.5
2.6
2.7
2.8
2.9
3
3.1
3.2
3.3
Density (g/cm3)

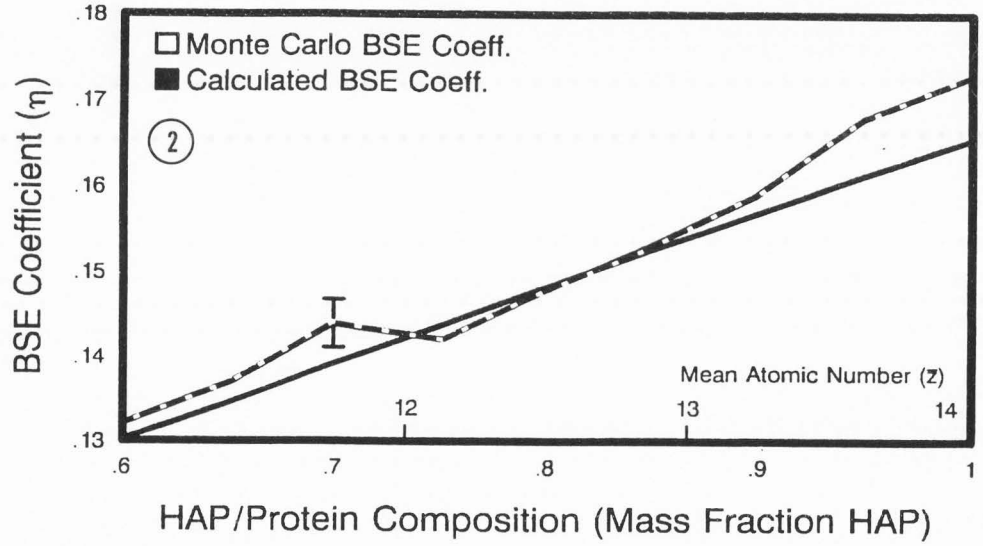
Monte Carlo BSE Coeff.
Calculated BSE Coeff.
2
Mean Atomic Number (z)
12
13
14
BSE Coefficient (η)
.18
.17
.16
.15
.14
.13
.6
.7
.8
.9
1
HAP/Protein Composition (Mass Fraction HAP)

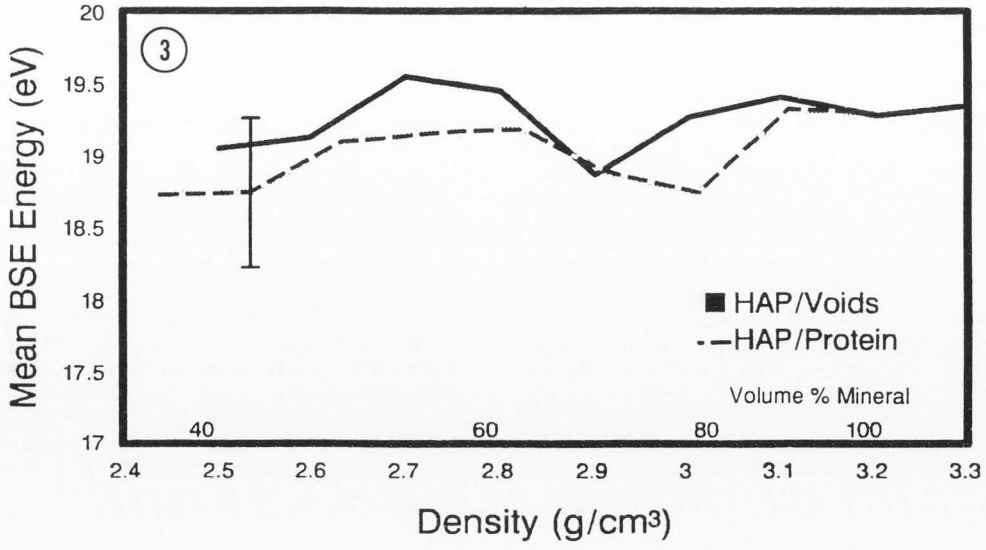
3
HAP/Voids
HAP/Protein
Volume % Mineral
40
60
80
100
Mean BSE Energy (eV)
20
19.5
19
18.5
18
17.5
17
2.4
2.5
2.6
2.7
2.8
2.9
3
3.1
3.2
3.3
Density (g/cm3)

Table. 3. Monte Carlo Calculations of HAP / 1.5 wt.% Protein Composite

Mass Fraction of HAP	Volume Fraction of HAP	Mean Atomic Number	Density g/cm^3	BSE Coefficient (±0.002)	Range (micrometers)
1.00	1.000	14.08	3.20	0.173	7.59
0.89	0.985	13.96	3.06	0.169	7.92
0.79	0.983	13.95	2.90	0.166	8.36
0.70	0.983	13.95	2.74	0.164	8.85
0.62	0.982	13.94	2.58	0.166	9.40
0.55	0.980	13.93	2.42	0.163	10.02
0.49	0.979	13.92	2.26	0.163	10.72
0.43	0.977	13.91	2.10	0.166	11.54
0.38	0.976	13.89	1.94	0.163	12.49

Table 4. Monte Carlo Calculations of Calcium Phosphate Phases

Phase	Mean Atomic Number	Mean Atomic Weight	Density g/cm^3	BSE Coefficient (±0.002)	Range (micrometers)
$Ca_{10}(PO_4)_6(OH)_2$	14.08	28.34	3.2	0.173	7.59
$Ca_3(PO_4)_2$	14.05	28.32	3.1	0.167	7.74
$Ca_9H(PO_4)_6OH.H_2O$	13.80	27.80	3.0	0.168	8.08
$Ca_8H_2(PO_4)_6.5H_2O$	13.51	26.50	2.8	0.158	8.59
$CaHPO_4.2H_2O$	11.85	23.86	2.3	0.146	10.24

Until now, we have been assuming in our models of demineralized enamel that the mineral component of enamel was stoichiometric HAP. However, the mineral component of enamel can best be described as a calcium-deficient carbonated apatite. Some theories of lesion formation suggest that highly-defective apatite is the first to dissolve (e.g., carbonated apatite) (Hallsworth et al., 1973) and that the reprecipitation of a more stoichiometric HAP occurs in other parts of the lesion. Others have suggested that under certain conditions phases such as brushite, $CaHPO_4.2H_2O$, (Brown et al., 1975; Featherstone et al., 1979) octacalcium phosphate (OCP), $Ca_8H_2(PO_4)_6.5H_2O$, and whitlockite, $Ca_3(PO_4)_2$, can form in intercrystalline spaces formed by partial demineralization. The results of Monte Carlo calculations (Table 4) show that some of these other phases, particularly brushite and OCP, do cause a reduction in the BE coefficient relative to HAP and that they may affect the BE images if these phases occurred in large concentrations (i.e., greater than 5 wt %) within the subsurface lesion. Defect apatites, including calcium-deficient apatites and carbonated apatites also have lower atomic numbers than pure HAP. If a defect apatite in sound enamel were to dissolve preferentially and precipitate as pure HAP or whitlockite, this would also affect the contrast in the BE images.

Experimental BE images of polished human enamel that had been demineralized in the intra-oral caries test, exhibited a mosaic pattern of prisms in cross-section when the exposed surface was viewed in BE mode in the SEM (Figs. 4 a-d). Enamel in the head and tail regions (i.e., prismatic and interprismatic) appeared to demineralize leaving a thin white rim, 0.5 to 1.0 micrometers wide at the prism peripheries. In those samples where demineralization appeared to be most severe the prism cores appeared uniformly dark (Fig. 4 a,d), while in other samples the prism heads were more blotchy (Fig. 4 b,c). In samples where the prism cores were darker, the prism peripheries appeared to be more pronounced.

When these samples were hemi-sectioned, the same lesions could be viewed longitudinally, extending from the exposed surface, through the demineralized enamel to underlying sound enamel (Figs. 4 e-h). Near the surface, the dark prism cores were delineated by white bands which presumably were the same white prism peripheries seen in Figs. 4 a-d. However, near the advancing front of the lesion, this pattern was reversed. Here the prism cores sometimes appeared to be whiter than those in the sound underlying enamel (Figs. 4 e,h), while in all cases the prism junctions, which normally can be discerned by a very thin dark line in BE images, were widened. Cross-striations approximately 3 micrometers apart were seen in one sample where the prisms were sectioned along their long axis. These lesions had not yet developed any indications of mineralized surface layers and could be considered as examples of "surface softening".

Natural subsurface lesions exhibited many of the features seen in artificial lesions including a well-mineralized surface zone, lesion body, striae of Retzius and details of prism microstructure (Fig. 5). At low magnification, a BE image of a typical natural

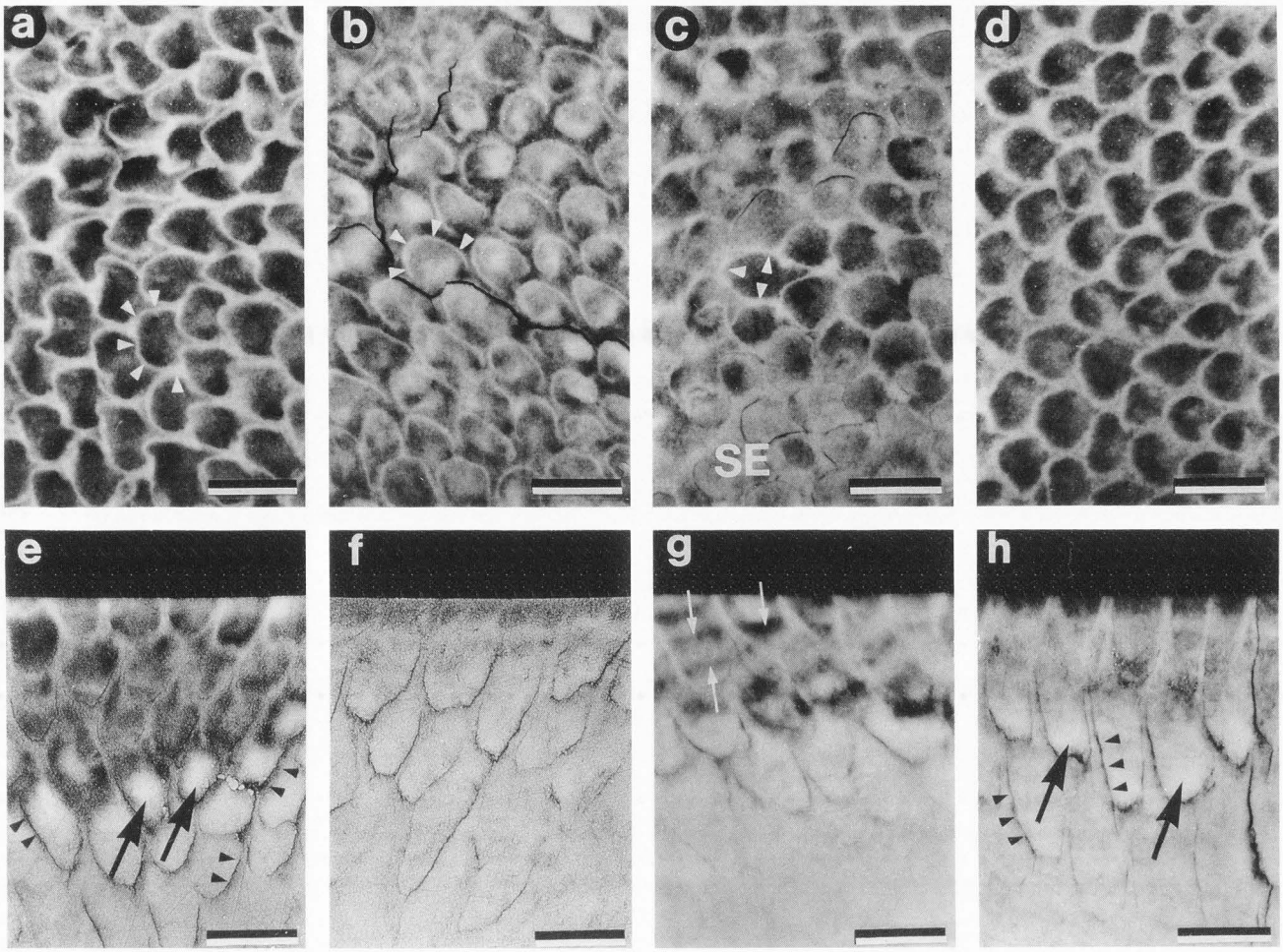

Figure 4. BE images of 4 lesions produced in the intra-oral appliance both in cross-section (a-d), and in longitudinal section (e-h). In c, SE denotes relatively sound enamel. White arrowheads in a,b,c denote remineralized, white, prism peripheries as opposed to dark prism cores. Black arrowheads in e,h denote widened prism junctions at the advancing lesion front. Large black arrows (e,h) show remineralized prism cores near advancing front. White arrows in g indicate cross striations. Bars = 10 micrometers. (Courtesy J. Dent. Res.).

lesion (Fig. 5 a) was very similar in appearance to a microradiograph of another lesion (Fig. 5 b). In the body of the lesion (Figs. 5 c,d,e), the prism peripheries appeared as white bands, which at high magnifications often contained a thin dark line, the prism junction. The prism cores were darker than the prism peripheries, although the contrast in the prism cores was very irregular along the length of the prisms. These bands of varying intensity traversed the prisms perpendicularly and were spaced approximately 2-4 micrometers apart. Adjacent prisms sometimes showed remarkable replication of the cross-striation patterns (Fig. 5 c, white arrows). Striae of Retzius were seen as dark bands diagonally traversing the lesion body, but the prisms at these regions were often widened as though the prisms were kinked or twisted. At the advancing front of the lesions (Fig. 5 f, labeled J), widened prism junctions could be seen between apparently unaffected prism cores. The underlying sound enamel was nearly featureless.

BE images (Fig. 6) of the transversely-sectioned lesions produced by a) a control, and each of three treatments, b) a NaF mouthwash with 225 ppm F, c) an MFP dentifrice with 1000 ppm F, d) a NaF dentifrice with 1100 ppm F, in an experiment using the pH cycling technique, showed clear differences in the depth of demineralization, the pattern of de- and remineralization and the intensity of demineralization (Fig. 6). The lesions were consistent with both microhardness and proton microprobe data not reported here. The control lesions were deeper than lesions produced with each of the three treatments confirming that each of these consumer products was efficacious. The surface layers in the control lesions were thinner than the treatment lesions. Lesions produced by the NaF dentifrice had the most mineralized or thickest surface layer and often had a striated appearance with several bands of alternating mineral density extending into the body of the lesion.

Lesions produced by the MFP dentifrice had shallow lesions with thinner surface layers than those produced by the NaF dentifrice or mouthwash. Lesions produced by the NaF mouthwash were similar

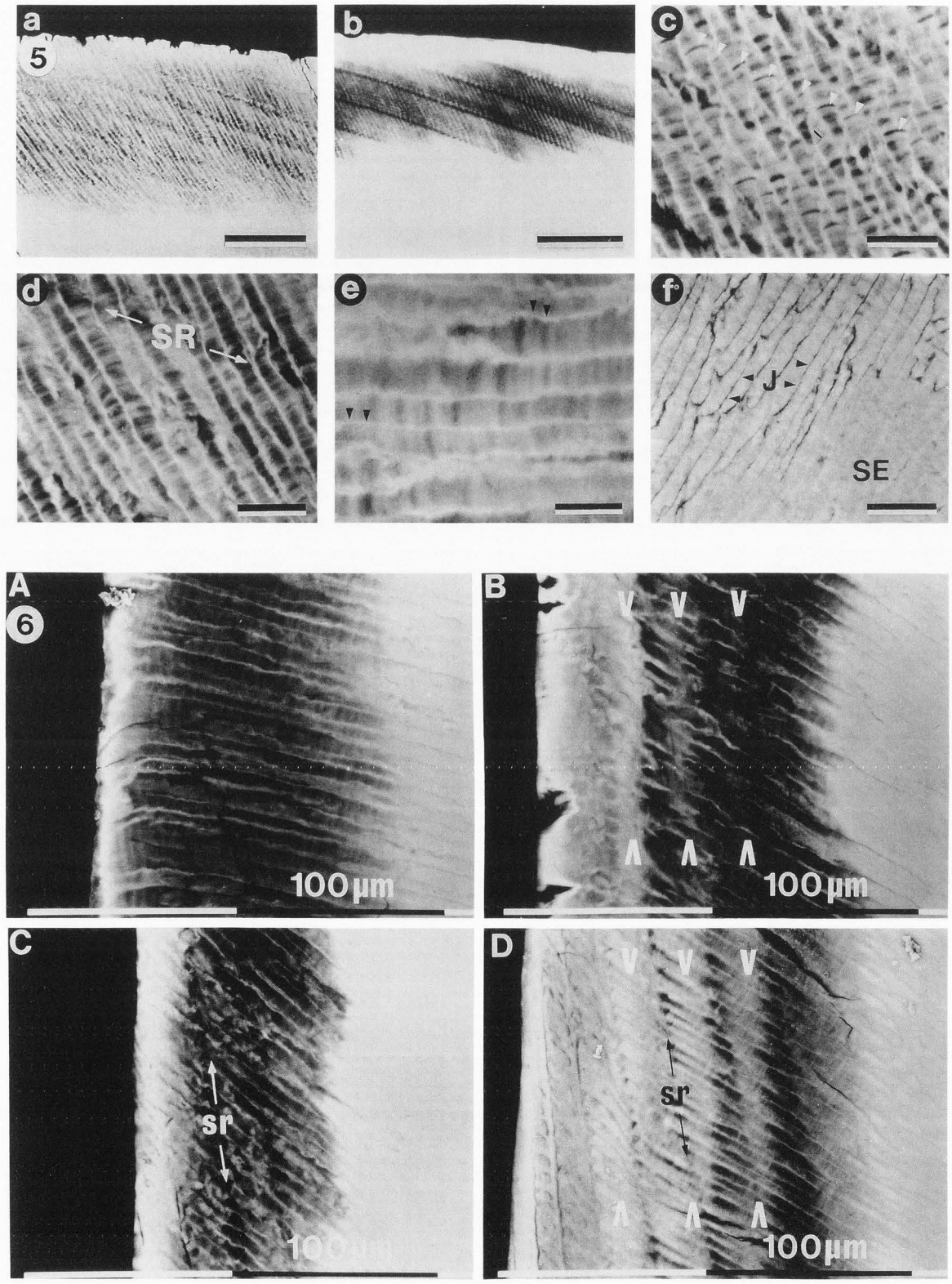

Figure 6. BE images of artificial lesions produced by the pH cycling model. a) is a control lesion, b) is a lesion produced by treatment with a NaF mouthwash, c) is a lesion produced by treatment with a monofluorophosphate dentifrice, and d) is a lesion produced by a NaF dentifrice. Notice the laminations in the lesions produced by the NaF mouthwash and dentifrice. Striae of Retzius are labelled sr.

Figure 5 (facing page, top). BE images (a,c-f) of natural lesions. Compare the similarities of a low magnification BE view of a lesion (a) with a microradiograph (b) of another natural lesion at the same magnification. Images c-e are higher magnification images of the lesion body, with striae of Retzius, SR, white prism peripheries and cross striations. At the advancing front of the lesions, widened prism junctions, J, and sound enamel, SE, could be seen. Bars: a,b = 100 micrometers; c,d,f = 20 micrometers; e = 10 micrometers. (Courtesy J. Dent. Res.).

to those of the NaF dentifrice, although they seemed more demineralized and had a thinner surface layer.

In another experiment, demineralization of enamel in an in vitro model was followed by BE imaging (Fig. 7). Polished enamel chips were withdrawn from a demineralizing solution (pH 4.5, 0.1 M lactate buffer with 0.2 mM MHDP as described above in Materials and Methods) after 1, 2, 6, 12 and 48 hrs. BE and SE images of the demineralized chips and control undemineralized chips were compared. For BE imaging, the BE detector amplifier gain, the beam current, the working distance, and the spot size were all kept constant for direct comparison. The photography parameters were also kept constant and the negatives were processed simultaneously so that the grey scales in the BE images could also be directly compared with each other. In the control enamel, mineral-rich (i.e., white) prism peripheries could just be seen, along with some scratch marks. However, after 1 hour of demineralization, the contrast between prism peripheries and prism cores had increased. Increased contrast between prism peripheries and cores seemed to occur as the period of demineralization increased. In fact, as demineralization continued, the prism cores became darker relative to the control implying local demineralization whereas the prism peripheries became whiter relative to the control implying local remineralization. Alongside each BE image is a corresponding SE image of the same enamel surface taken at higher magnification. These SE images show a gradual opening up of inter-crystalline spaces as demineralization continued.

Discussion

There is an extraordinary similarity between low magnification BE images and microradiographic images of partially-demineralized enamel. For example, both techniques show striae of Retzius, surface layers and in the body of the lesion, prism cross-striations with mineral-deficient prism cores surrounded by mineral-dense rims. Many previous reports (Boyde and Jones, 1983; Jones and Boyde, 1987; Pearce and Nelson, 1989) have assumed that the BE images of demineralized enamel "represent" or "reflect" variations in enamel mineral density. However, the Monte Carlo calculations show that simple variations in HAP density cannot alone account for the contrast seen in the BE images of demineralized enamel because even though the primary electron range increases with decreasing density, the BE coefficient is unaffected. These calculations are a good simulation of a densely-packed HAP ceramic that has been demineralized. Such a demineralized ceramic is predicted to show no contrast in BE images, whereas a lesion in such a material can be "seen" by microradiography.

Another set of calculations based on a model consisting of HAP and protein where the relative proportion of HAP to protein decreased from 100/0 to 38/62 did show corresponding significant decreases in the BE coefficient. Dentin appears darker than enamel in BE images and the calculations confirm that the reason lies in the fact that the mean atomic number of enamel (87% mineral by volume) is approximately 13.7 whereas for dentin (45% mineral by volume) it is approximately 11.5. Therefore, the differing contrast in BE images of these two materials is due to changes in mean atomic number arising from the increased proportion of protein relative to mineral in dentin.

Enamel, however, contains on average only 1.5 wt % of organic matter, 95 wt % apatite and the remaining 3.5 wt % is water. The mass fraction of apatite in dehydrated enamel is approximately 0.985. If we assume that during subsurface lesion formation only the apatite phase dissolves and no protein is lost, the mass fraction of apatite will decrease slightly as more mineral phase is lost. When the volume fraction of HAP reaches 0.38, comparable to that found in a well-demineralized lesion, the mass fraction dropped to 0.976 and there was little, if any, change in the calculated BE coefficient, even though the density dropped from 3.06 to 1.94 g/cm^3. Initially, this set of calculations was puzzling because it did not appear to explain the contrast in the BE images. However, the calculated mean atomic number dropped by 0.07, so in theory the BE coefficient should decrease slightly. It is well known that changes of $\bar{Z}=1$ can very easily be seen in elements with high atomic number where the $\bar{Z}$ verses BE coefficient curve is relatively flat. Therefore, it seems reasonable that changes as small as $\bar{Z}=0.1$ could be observed in the small atomic number region.

Boyde (1979) suggested that cross-striations were the result of rhythmic variations in the ratio of carbonate to phosphate in the dental mineral and that this may the reason for their appearance in BE images. On the other hand, Simmelink and Nygaard (1982), using TEM, have shown that crystals in the region of cross-striations in demineralized enamel are smaller and fewer in number. In the experiment where the formation of a subsurface lesion was studied using BE imaging, it appeared that the prism peripheries became whiter (i.e., BE coefficient increased) as the lesion progressed while the prism cores became darker (i.e., BE coefficient decreased). It is interesting to note that in sound enamel the prism peripheries were already slightly whiter compared to the prism cores suggesting that local variations in the mineral/protein ratio occur at the prism microstructural level. Enamel produces etching patterns under certain conditions that may be due to a similar phenomenon.

For example, unstirred organic acids produce a type 1 etch pattern on enamel where the prism peripheries are elevated above the prism cores and sometimes above neighboring unetched enamel. This indicates that reprecipitation of dissolved material at prism peripheries seems to cause the ridges of the "honeycomb" appearance of type 1 etch pattern.

From these previous observations and the difficulty in explaining the contrast in BE images using

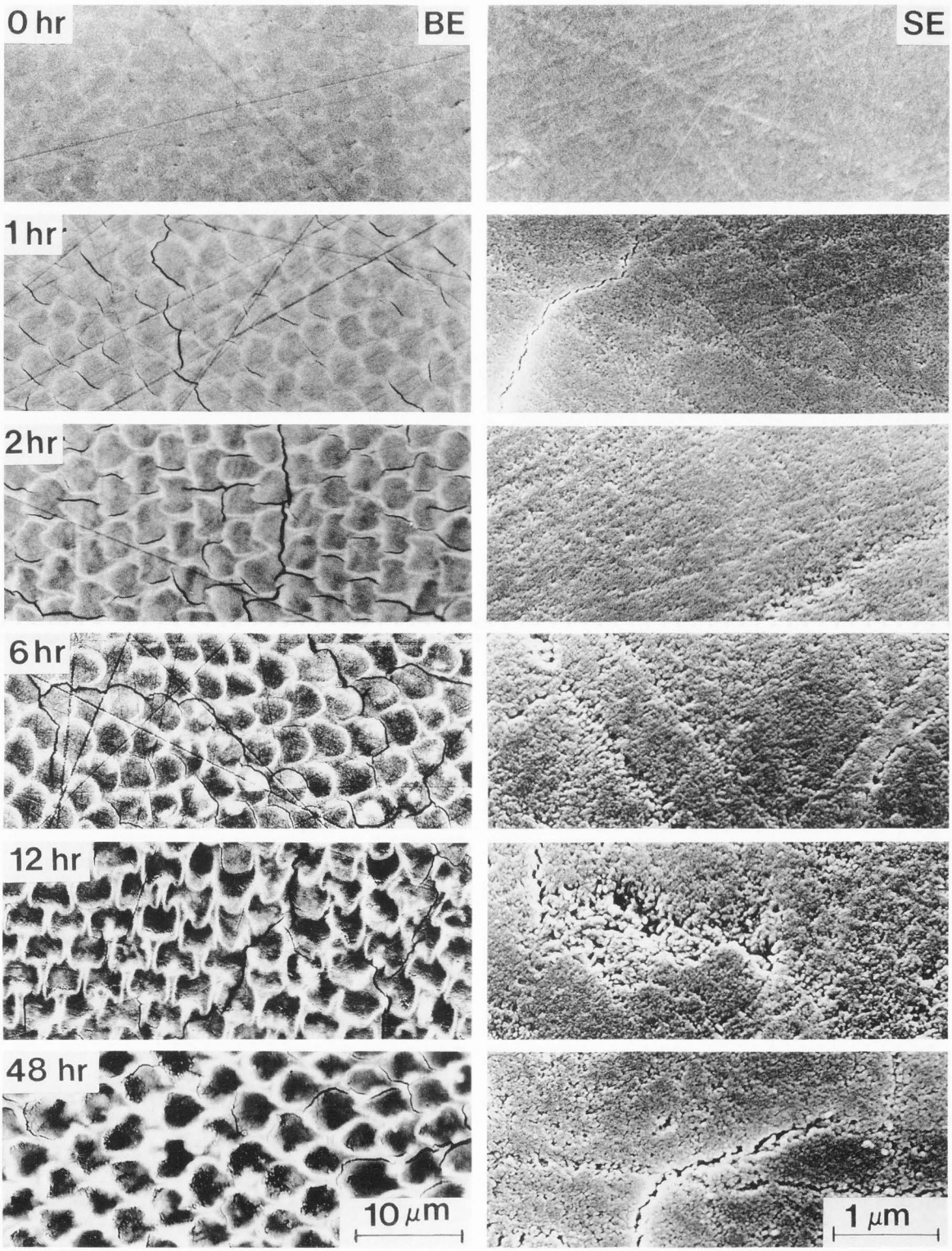

Figure 7. BE images (left side) and high magnification SE images (right side) of an artificial lesion produced by a demineralizing solution consisting of pH 4.5, 0.1 M lactate buffer with 0.2 mM MHDP forming in polished human enamel. Images were taken after 0, 1, 2, 6, 12 and 48 hrs. In the BE images, prism peripheries became whiter and prism cores became darker. In the SE images, small intercrystallite pores "opened up" as demineralization continued.

models described above, other mechanisms must be responsible for the contrast in the images. We propose two possible mechanisms. The first is that there are local variations at prism level in the protein/mineral ratio and/or that there are local variations in the reactivity of enamel which lead to local variations in the protein/mineral ratio in demineralized enamel when compared to sound enamel. Any large increase in the protein/mineral ratio will cause a change in the BE coefficient. The second mechanism suggests that the precipitation of other calcium phosphate phases may account for the contrast seen in the BE images. Two possibilities exist: 1) Reprecipitation of crystals with a low $\bar{Z}$ such as brushite or OCP could occur giving rise to dark areas in the BE images; or 2) Reprecipitation of a more perfect HAP phase or whitlockite phase with a higher $\bar{Z}$ giving rise to whiter areas in the BE images. Sound enamel crystals are known to be calcium-deficient carbonated apatites, and if a phase such as this were to dissolve and reprecipitate as a near stoichiometric HAP, the $\bar{Z}$ would increase by 0.2 - 0.3 which would result in an increase in the backscatter coefficient of approximately 2%.

Therefore, in sound enamel, a possible explanation for features such as cross-striations and the striae of Retzius may be that there are local regions with a higher protein/mineral ratio than the average and this gives rise to the contrast in BE images. In demineralized enamel, crystals in these regions may preferentially dissolve, enhancing the difference in protein/mineral ratio between mineral dense and mineral deficient regions. Other microstructural features, such as the "white" prism peripheries, although containing a lower mass fraction of organic matter than the prism cores in sound enamel, become whiter in demineralized enamel because of the reprecipitation of higher $\bar{Z}$ calcium phosphate phases and perhaps some protein could be lost from the prism peripheries. The prism cores become darker because apatite crystals dissolve leaving organic matter behind, thus increasing the protein/mineral ratio. Prism junctions appear black relative to prism peripheries because they consist of a small "gap" presumably filled with organic matter where crystal orientations abruptly change. Widening of the prism junctions at the advancing front of the lesion suggests that acid penetrates underlying sound enamel via prism junctions. This occurs even though the entire enamel surface is porous, and prism cores eventually become the most demineralized prism feature in the body of the lesion.

The future of this technique, in conjunction with microradiography, looks promising. Presently we are considering the construction of a microstepwedge consisting of materials with $\bar{Z}$'s between 11-14 so that we can digitize BE images and quantify re- and demineralization processes in demineralized enamel during subsurface lesion formation.

Acknowledgments

I would like to thank Dr. Euan Pearce, Dental Research Unit, Wellington, New Zealand and Dr. Ron Warner, Miami Valley Labs, The Procter and Gamble Company, for their help in preparing this paper. Dr. David Joy, EM Facility, University of Tennessee is thanked for making the program used in this paper available.

References

Arends J, Gelhard TBFM (1983) In vivo remineralization of human enamel; in Leach, Edgar, Remineralization and demineralization of the teeth, pp. 1-16 (IRL Press, Oxford).

Boyde A (1979) Carbonate concentration, crystal centers, core dissolution, caries, cross striations, circadian rhythms, and compositional contrast in the SEM. J. Dent. Res. Special Issue B 981-983.

Boyde A, Jones SJ (1983) Backscattered electron imaging of dental tissues. Anat. Embryol. 168 211-226.

Brown WE, Patel PR, Chow LC (1975) Formation of $CaHPO_4.2H_2O$ from enamel mineral and its relationship to caries mechanism. J. Dent. Res. 54 475-481.

Featherstone JDB, Duncan JF, Cutress TW (1979) A mechanism for dental caries based on chemical processes and diffusion phenomena during in-vitro caries simulation on human tooth enamel. Archs Oral Biol. 24 101-112.

Groeneveld A (1974) Dental caries: some aspects of artificial carious lesions examined by contact microradiography. PhD Thesis, University of Utrecht, Holland.

Hallsworth AS, Weatherell JA, Robinson C (1973) Loss of carbonate during the first stages of enamel caries. Caries Res. 7 345-348.

Jones SJ, Boyde A (1987) Scanning microscopic observations on dental caries. Scanning Microsc. 1 1991-2002.

Joy DC (1988) An introduction to Monte Carlo simulations. Inst. Phys. (Bristol, U.K.) Conf. Ser. No. 93 23-32.

Pearce EIF, Gallagher IHC (1979) The behavior of sucrose and xylitol in an intra-oral caries test. NZ Dent J. 75 8-14.

Pearce EIF, Nelson DGA (1989) Microstructural features of carious human enamel imaged with backscattered electrons. J. Dent. Res. 68 113-118.

Reuter W (1972) The ionization function and its application to the elctron probe analyssi of thin films. In: Proceedings of the Sixth International Conference on X-ray Optics and Microanalysis, Shinoda G, Kohra K, Ichinokawa T (eds.), University of Tokyo Press, Japan, 121-130.

Shellis RP, Hallsworth AS (1987) The use of scanning electron microscopy in studying enamel caries. Scanning Microsc. 1 1109-1123.

Silverstone LM (1973) Structure of carious enamel, including the early lesion. Oral Sci. Rev. 3 100-160.

Silverstone LM (1977) Remineralization phenomena. Caries Res. 11 (Suppl. 1.) 59-84.

Simmelink LM, Nygaard VK (1982) Ultrastructure of striations in carious human enamel. Caries Res 16 179-188.

Takagi S, Chow LC, Brown WE, Dobbyn RC, Kuriyama M (1984) Parallel beam microradiography of dental hard tissue using synchrotron radiation and X-ray image magnification. Nucl. Instr. Meth. 222 256-258.

White DJ (1988) Reactivity of fluoride dentifrices with artificial caries II. Effects on subsurface lesions: F uptake, F distribution, surface hardening and remineralization. Caries Res 22 27-36.

Discussion with Reviewers

R.P. Shellis: It is suggested that the low electron emission by dentin, and hence the high contrast between dentin and enamel, is due to the low value of $\bar{Z}$. Therefore, it would be predicted that if a section containing enamel and dentin is deproteinized using hypochlorite or ethylenediamine, the emission by dentin should increase and the contrast between enamel and dentin be reduced.

Author: It is correct that if a true anorganic specimen containing both enamel and dentin could be prepared, the high contrast between enamel and dentin would be greatly reduced because both materials would now have similar mean atomic numbers. We checked this experimentally by extracting epoxy-embedded hemi-sectioned human teeth with neutral 10% NaOCl to remove protein and then a 3:1 chloroform: methanol mixture to remove lipids. BE images of extracted teeth had greatly-reduced contrast, as predicted, between the enamel and dentin than intact specimens. We believe that most of the residual contrast is due to incomplete extraction of all organic matter from dentin, especially several micrometers beneath the sectioned surface.

R.P. Shellis: If such an anorganic specimen were then to be infiltrated with methyl methacrylate (mean atomic number = 3.6), the emission should again decrease and the enamel/dentin contrast increase. It might also be possible to visualize the dentinal tubules in such specimens, through the difference in mean atomic numbers.

Author: The trouble with infiltrating a resin into an anorganic specimen of enamel and dentin is the very friable nature of the specimen. This makes it extremely difficult, if not impossible to do. Dentinal tubules surrounded by annular, more highly-mineralized peritubular dentin are visualized in BE images of polished, intact or demineralized dentin. In this case, the tubules are seen because of topographical contrast mechanisms whereas the peritubular dentin has a higher mean atomic number than intertubular dentin.

R.P. Shellis: Similar manipulations could be done on low contrast specimens of slightly demineralized enamel (e.g., the top 2 specimens of Fig. 7), to explore the contrast mechanism actually in carious enamel.

Author: Polished enamel sections of artificial lesions that had been extracted with NaOCl and chloroform: methanol again had greatly reduced contrast when compared with unextracted controls. Samples extracted this way clearly show that it is protein/mineral ratio, and not density, which determines the BE coefficient and, hence, the contrast in BE images of enamel.

A. Boyde: Was the contribution of the epoxy embedding resin ignored in the Monte Carlo calculations?

Authors: The epoxy resin that was used was not infiltrated into the hemi-section surfaces of transversely-sectioned lesions and did not diffuse through the anatomical surface of the enamel into subsurface enamel. Consequently, the resin was not relevant for the calculations. Sectioned teeth were embedded in resin merely to provide support for polishing for subsequent SEM examination. Similarly, prepolished enamel chips also were not infiltrated with resin.